Antenna Mutual-Coupling Mitigation With Analogue Compensation Network

Roger Green[#1], Tommaso A. Cappello[#2], Geoff Hilton[#3] Mark Beach[#4]
[#]Department of Electrical and Electronic Engineering, CSN Laboratory, UK
{[1]roger.green, [2]tommaso.cappello, [3]geoff.hilton, [4]m.a.beach}@bristol.ac.uk

***Abstract* — This work presents a systematic approach supported by theory, simulation, and measurements that demonstrates antenna mutual-coupling reduction by means of an analogue compensation network. This compensation network is realized with two couplers and a passive network based on a 2^{nd}-order band-pass filter. A 3.5 GHz two-element patch antenna is built and used for comparison with the same antenna and compensation network. After a theoretical analysis highlighting the relevant design constraints, simulated and measured results demonstrate a reduction in the antenna $|S_{A12}|$ from -27 dBs to -50 dBs, corresponding to an improvement up to 23 dB over the whole antenna -10 dB bandwidth, while the antenna S_{A11} and S_{A22} remain unchanged. This $|S_{A12}|$ improvement is also shown to improve the far-field radiation pattern for the considered antenna array.**

***Keywords* — antenna array, antenna isolation, decoupling network, MIMO, mutual coupling, vector cancellation.**

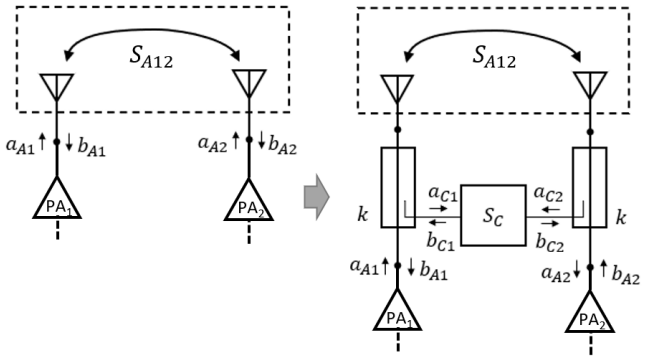

Fig. 1. Left: antenna mutual-coupling problem due to S_{A12}. Right: presented architecture for the cancellation of the mutual coupling using an auxiliary compensation network S_C here implemented as a band-pass filter.

I. Introduction

Antenna arrays are widely used in multiple-input multiple-output (MIMO), phased arrays and radar applications [1]. In such applications, each antenna element may have a different amplitude/phase weighting and transmitted signal. Retaining independence from the signal being transmitted on other antenna elements is necessary [2] for high-speed data transmission, predictable beam steering and spatial diversity (required for MIMO). However, electromagnetic coupling introduces increasing correlation between the elements as the inter-element distance reduces. A widely spaced array may require a physically large enclosure and may not always be feasible. With closely spaced antenna elements, mutual coupling causes one antenna to irradiate all the others, with the closest elements most affected [1]. Beam forming, far-field radiation pattern [3], power-amplifier (PA) linearity and the overall communication link capacity are all adversely affected by antenna mutual coupling [4]–[8]. The PA, being the last element before the antenna, can suffer from (active) load-pulling effects [5] due to the coupled signals which can alter its amplification characteristics. Isolators can be introduced between the PA and the antenna to terminate the reflected/coupled wave(s) but these components are bulky, narrowband, lossy and difficult to integrate.

Digital and analogue techniques are proposed in the literature to mitigate the mutual coupling problem in closely-spaced antenna arrays. Digital techniques are based on digital pre-distortion (DPD) of the input signal to compensate for the load variation due to the coupled signals [5]–[7]. However, in this approach the DPD needs to account for all the other signals in the other branches (e.g. 2-D memory polynomial). This is challenging for large arrays due to the computational complexity, latency and cost. Instead, analogue techniques can directly mitigate this issue as part of the antenna design and depending on their implementation, they can be summarized as: electromagnetic band-gap methods [9], parasitic antennas [10], coupled resonators [11], and a secondary decoupling surface [12]. However, all these methods are not able to provide wide bandwidths or scan angle and cannot be seamlessly scaled up into large antenna arrays.

In this work, a novel, systematic technique for reducing antenna coupling is presented. This technique is demonstrated for a two-element patch antenna array and its block diagram is shown in Fig. 1. After a theoretical analysis of the problem, a compensation network is designed and used to demonstrate the cancellation of the antenna $|S_{A12}|$.

II. Theory of Antenna Cross-Coupling Mitigation

When two different signal waves $[a_{A1}, a_{A2}]$ excite a pair of coupled antennas, the reflected wave can be calculated as

$$\begin{cases} b_{A1} = S_{A11}a_{A1} + S_{A12}a_{A2}, \\ b_{A2} = S_{A21}a_{A1} + S_{A22}a_{A2}. \end{cases} \tag{1}$$

In the following, the contribution of S_{A11} and S_{A22} is not considered as they cause a modification of the load impedances dependent on the amplified signal (respectively a_{A1} to b_{A1} and a_{A2} to b_{A2}). Instead, the cross-modulation terms $S_{A12} = S_{A21}$ mix the two signals and so a_{A1} affects the PA$_2$ and a_{A2} affects the PA$_1$ and this is the key issue in cross-coupled antennas. In fact, the reflected wave $[b'_{A1}, b'_{A2}]$ due to cross-modulation

modifies the PA load impedances in a non-predictable manner. The reflected waves due to the coupled signals are

$$b'_{A1} = S_{A12} \cdot a_{A2}, \qquad b'_{A2} = S_{A21} \cdot a_{A1}, \tag{2}$$

The proposed solution is illustrated as follows. Let's introduce an ideal RF directional coupler before the antenna ports with coupling factor $\mathrm{CF}\,(\mathrm{dB}) = 20\log_{10}(|k|)$, where k is a complex coupling parameter. These couplers (one for each antenna) sense the incident waves $[a_{A1}, a_{A2}]$ and they generate the coupled waves

$$a_{C1} = k \cdot a_{A1}, \qquad a_{C2} = k \cdot a_{A2}. \tag{3}$$

Connected to the coupled ports, a two-port network is introduced as in Fig. 1 and described by

$$\begin{bmatrix} b_{C1} \\ b_{C2} \end{bmatrix} = \begin{bmatrix} 0 & \alpha_C \\ \alpha_C & 0 \end{bmatrix} \cdot \begin{bmatrix} a_{C1} \\ a_{C2} \end{bmatrix} = k \cdot \begin{bmatrix} 0 & \alpha_C \\ \alpha_C & 0 \end{bmatrix} \cdot \begin{bmatrix} a_{A1} \\ a_{A2} \end{bmatrix} \tag{4}$$

The condition required for cancelling out the cross-coupled waves at the coupler input interface is

$$\begin{bmatrix} b'_{A1} \\ b'_{A2} \end{bmatrix} - k \cdot \begin{bmatrix} b_{C1} \\ b_{C2} \end{bmatrix} = \begin{bmatrix} 0 \\ 0 \end{bmatrix} \tag{5}$$

After replacing (1) and (4) in (5), it results

$$S_{A12} = S_{A21} = \alpha_C \cdot k^2. \tag{6}$$

This complex-valued equation establishes a relationship to provide cross-coupling cancellation for a two-element antenna with S_{A12} parameter. Choosing the appropriate α_C and k value affects the performance of the compensation network. In a coupler, the coupling loss increases with k, and therefore it is necessary to minimize $|k|$ and maximize $|\alpha_C|$ in (6) while ensuring the product is equal to S_{A12}, both in amplitude and phase. We note that this strategy is also effective as k appears as a quadratic term in (6). We also point out that the couplers could be used to feed back the PA output signal for DPD.

III. Design of the Compensation Network

Two closely-spaced patch antenna elements are designed and used as a benchmark against the same antenna pair with the compensation network. Initial antenna geometries are obtained from the formulae in [1] and successively, the antenna is optimized using Keysight ADS. The antenna is centered at $f_C = 3.475\,\mathrm{GHz}$ and with a $-10\,\mathrm{dB}$ bandwidth $\mathrm{BW} = f_H - f_L = 70\,\mathrm{MHz}$ ($f_L = 3.44\,\mathrm{GHz}$ and $f_H = 3.51\,\mathrm{GHz}$). This results in a prototype of Fig. 7(left) whose width is 25.6 mm, height of 20.6 mm, and a slot of 3.5 mm wide and 3.2 mm deep. The antenna feed lines are separated by a 58 mm distance. Fig. 2 shows the antenna simulated S-parameters. Here, the $|S_{A12}|$ rises in frequency and peaks at $-24.2\,\mathrm{dB}$ at the resonance f_C and it then decays within the bandwidth.

Fig. 3 shows the target S_{A12} in amplitude and phase that need to be matched to the coupler-compensation network block. We observe that the general shaping of $|S_{A12}|$ is similar to the response of a band-pass filter (BPF) and this is the design method used for the compensation network which can be summarized as follows:

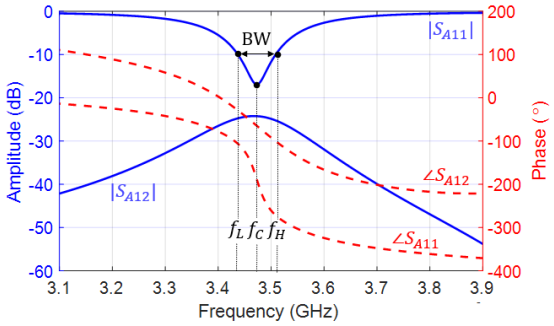

Fig. 2. Simulated antenna S-parameters and -10 dB bandwidth definition.

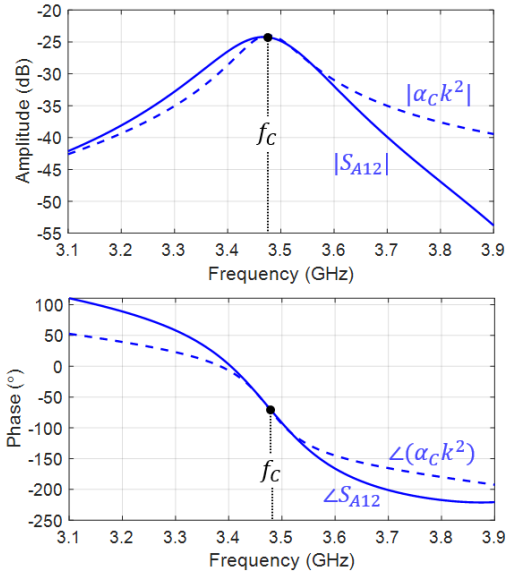

Fig. 3. Amplitude (top) and phase (bottom) of the antennas with couplers (solid line) and of the band-pass filter compensation network (dotted line). The design of the compensation network is optimized according to (6).

Antenna Coupling $\lvert S_{A12}\rvert$	Required Coupling Factor (CF)	Coupler Insertion Loss (Ideal)
16 dB	8 dB	0.75 dB
20 dB	10 dB	0.46 dB
24 dB ←	**12 dB ←**	**0.28 dB ←**
28 dB	14 dB	0.18 dB
32 dB	16 dB	0.11 dB

Fig. 4. Table reporting the antenna coupling $|S_{A12}|$ and the required coupling factors for $\alpha_C = 1$ and associated coupling losses. The arrow (←) indicates the choice for this work.

1) Design a band-pass filter centred at f_C to match the antenna S_{A12} within the antenna bandwidth BW (both in amplitude and phase). To minimize coupling losses, the filter attenuation α_C at f_C has to be minimized.
2) Design a directional coupler with coupling factor $\mathrm{CF}\,(\mathrm{dB}) = (-|S_{A12}| - \alpha_C)/2$ in the antenna bandwidth BW. Account for the extra phase delay introduced by the coupler by tuning the BPF phase accordingly.

In this work, the BPF is implemented as a single coupled microstrip line whose geometries are depicted in Fig. 6. The filter is preliminarily designed using the formulas of [13] and

they result in a characteristic admittance of the J-inverter

$$J_{01} = \sqrt{\frac{\pi\Delta}{2g_0g_1}} = 0.125. \tag{7}$$

Here, $\Delta = (f_H - f_L)/f_C = 0.02$ is the fractional bandwidth, $g_0 = 1$ and $g_1 = 2$ are the elements of a Butterworth prototype filter derived from [13]. From (7), the odd- and even-mode characteristic impedances of the resonators are determined by

$$\begin{aligned}(Z_{0o})_{01} &= Z_0\left(1 - J_{01} + {J_{01}}^2\right) = 44.5\,\Omega \\ (Z_{0e})_{01} &= Z_0\left(1 + J_{01} + {J_{01}}^2\right) = 57.0\,\Omega.\end{aligned} \tag{8}$$

With a substrate thickness of 1.5 mm and relative dielectric constant $\epsilon_r = 4.3$, the initial spacing, widths, and lengths are evaluated. Successively, ADS simulations are performed to fine-tune the geometries, and resulting in the response of Fig. 5. For this BPF, the attenuation is 1.7 dB and the phase is $-72.8°$, or $\alpha_C = 0.82e^{-j72.8°}$.

Regarding the couplers, a coupling factor CF = 11.25 dB is required to satisfy (6), because $2 \times 11.25 + 1.7\,\text{dB} = 24.2\,\text{dB} = -|S_{A12}|$. From ADS simulations, the basic coupler geometry of Fig. 6 is determined, with spacing between lines of $S_1 = S_2 = 1.36$ mm, a line widths $W_1 = W_2 = W_3 = W_4 = 2.79$ mm, and an overall length of the single resonator of $L = 22.4$ mm (approximately $2 \cdot \lambda_C/8$). In this design, a 50-Ω resistor is used on the isolation port of the coupler. Finally, it is necessary to compensate the BPF for the extra phase delay introduced by the couplers (1.4°) and also from the necessary line lengths for physical interconnection.

Two in-house manufactured PCB boards are produced, using an 1.5-mm thick FR4 substrate with a relative dielectric constant $\epsilon_r = 4.3$ and 70-μm copper thickness. On the underside, there is an uninterrupted ground plane. One PCB contains just the antenna pair Fig. 7(left), the other, the pair with the compensation network Fig. 7(right).

With regard to the prototype manufacturing, the line lengths to the antenna and to the BPF are critical to the design and this is achieved with a tolerance of 0.1 mm with the current PCB process. From sensitivity analysis in ADS, both the amplitude and phase are required to match to 1 dB and 1° tolerance over the bandwidth. A 0.1 mm track length results in a phase delay of 0.75° at f_C which confirms the suitability of the PCB process. On the PCB with the compensation network, two parallel 100 Ω resistors are connected to the isolation port of the couplers, thus creating a 50 Ω termination.

IV. Experimental Results

Simulation results using Keysight ADS for the uncompensated and compensated antennas are reported in Fig. 8(top). When no compensation is used, the antenna $|S_{A12}|$ peaks at -24.2 dB at $f_C = 3.475$ GHz. With the compensation, a reduction to -56 dB is noted, thus providing an improvement of 31.8 dB (simulated).

The prototypes as displayed in Fig. 7 are measured using a Rohde & Schwarz ZNBT-8 20 port, 8.5 GHz vector network analyser, once calibrated using the Rohde & Schwarz

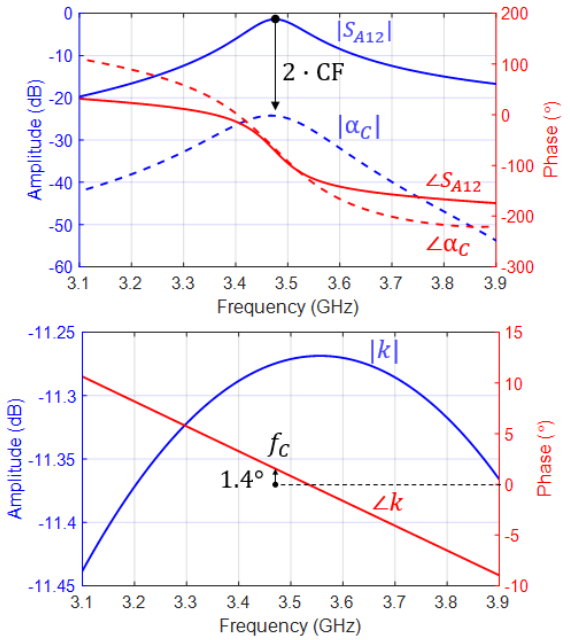

Fig. 5. S-parameters for the band-pass filter (top) and for the coupler (bottom). The filter has to introduce minimal attenuation and a phase rotation to match the antenna S_{A12} with the remaining attenuation introduced by the coupler.

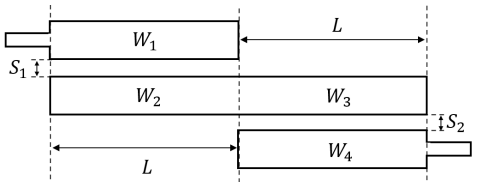

Fig. 6. Basic geometries of the considered coupled-line band-pass filter.

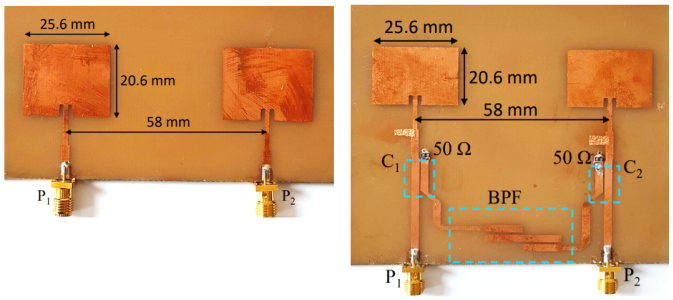

Fig. 7. Left: reference antenna. Right: reference antenna with compensation network. Here, two identical couplers C_1 and C_2 are connected to a compensation network that is here implemented with a band-pass filter (BPF).

ZN-Z51 calibration kit. The measured results are shown in Fig. 8(bottom). We note a reduction of the $|S_{A12}|$ from -27 dB to -50 dB (peak min), corresponding to an improvement of 23 dB (measured). We also observe that the $|S_{A11}| \cong |S_{A22}|$ are practically unchanged. When passing from simulations to measurements, the resonance frequencies of the patches and the cancellation network increases from 3.475 to 3.5 GHz, and this is most likely due to physical parameter variations (e.g., ϵ_r or substrate/copper thicknesses). This frequency variation is acceptable considering $f_C = 3.5$ GHz. In the prototype, additional tuning stubs are introduced on the antenna feed lines

using copper tape to achieve comparable $|S_{A11}|$ and $|S_{A22}|$ of the uncompensated case. We note the simulation did not require those tuning stubs and their presence compensates for materials characteristics differing from that is used in ADS.

The measured S-parameters are then used in Keysight's SystemVue in place of the antenna simulation model. A simulation is then performed to extract the radiation plot with 0 degree beam steer at $\lambda/2$ and isotropic radiation pattern (for the antenna elements), and the results are shown in Fig. 9. It can be seen that the compensated design improves null depth w.r.t the uncompensated.

V. Conclusion

This work presents a systematic approach supported by theory, simulation, and measurements that demonstrate antenna mutual-coupling compensation by means of an analogue compensation network. This method, when applied to a pair of patch antennas provides decoupling using a 2^{nd}-order coupled microstrip band-pass filter for the passive network. The measured $|S_{A12}|$ reduction is 23 dB and provides decoupling across the whole antenna bandwidth. This reduction in the mutual coupling is shown to improve the far-field radiation pattern for enhanced beam steering, data throughput and angle/spatial diversity. This methodology can be applied on multiple element single or two-dimensional antenna arrays, and this is the object of ongoing research.

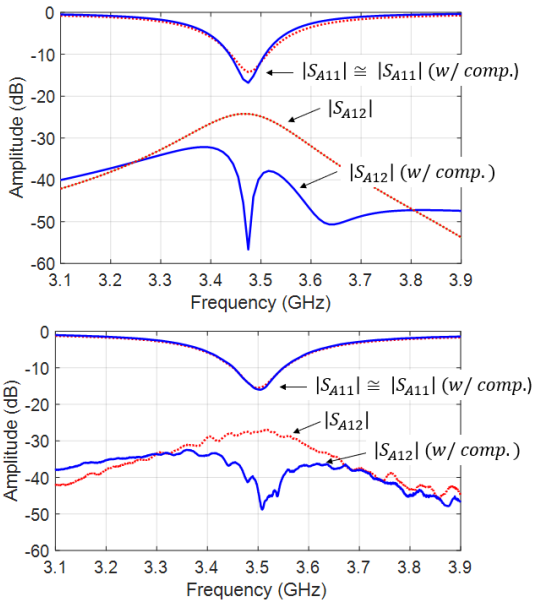

Fig. 8. Simulated (top) and measured (bottom) S-parameter amplitude for the un-compensated (red dotted) and compensated (blue solid) case. A slight frequency shift $f_C = 3.5$ GHz is found in the measured antenna which is however compensated with over 20 dB improvement on the $|S_{A21}|$ when the proposed compensation network is used.

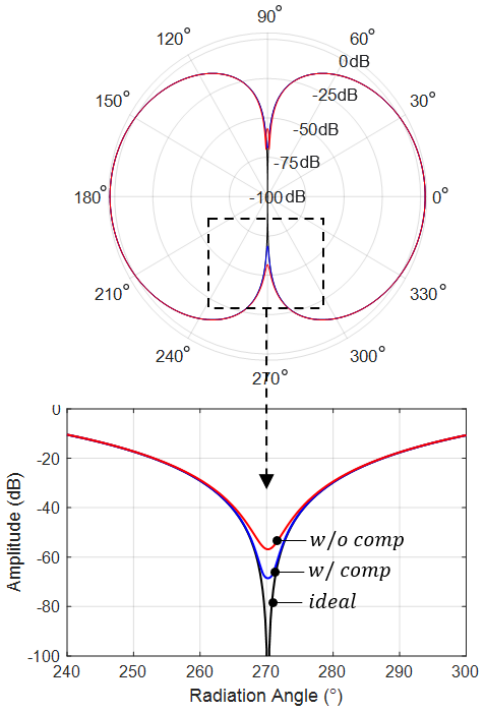

Fig. 9. Antenna radiation polar (top) and rectangular (bottom) plot obtained from measured S-parameters. In this last plot, it is shown the detail of the null suppression with the compensation network.

References

[1] C. A. Balanis, *Antenna Theory: Analysis and Design*. USA: Wiley-Interscience, 2005.

[2] F. Rusek, D. Persson, B. K. Lau, E. G. Larsson, T. L. Marzetta, O. Edfors, and F. Tufvesson, "Scaling up mimo: Opportunities and challenges with very large arrays," *IEEE Signal Process. Mag.*, vol. 30, no. 1, 2013.

[3] M. Romier, A. Barka, H. Aubert, J.-P. Martinaud, and M. Soiron, "Load-pull effect on radiation characteristics of active antennas," *Antennas Wireless Propag. Lett.*, vol. 7, pp. 550–552, 2008.

[4] C. Fager, K. Hausmair, K. Buisman, K. Andersson, E. Sienkiewicz, and D. Gustafsson, "Analysis of nonlinear distortion in phased array transmitters," in *2017 Integrated Nonlin. Microw. Mm-wave Circ. Workshop (INMMiC)*, 2017, pp. 1–4.

[5] F. M. Barradas, P. M. Tomé, J. M. Gomes, T. R. Cunha, P. M. Cabral, and J. C. Pedro, "Power, linearity, and efficiency prediction for mimo arrays with antenna coupling," *IEEE Trans. Microw. Theory Techn.*, vol. 65, no. 12, pp. 5284–5297, 2017.

[6] K. Hausmair, P. N. Landin, U. Gustavsson, C. Fager, and T. Eriksson, "Digital predistortion for multi-antenna transmitters affected by antenna crosstalk," *IEEE Trans. Microw. Theory Techn.*, vol. 66, no. 3, pp. 1524–1535, 2018.

[7] S. K. Dhar, A. Abdelhafiz, M. Aziz, M. Helaoui, and F. M. Ghannouchi, "A reflection-aware unified modeling and linearization approach for power amplifier under mismatch and mutual coupling," *IEEE Trans. Microw. Theory Techn.*, vol. 66, no. 9, pp. 4147–4157, 2018.

[8] T. Cappello, A. Duh, T. W. Barton, and Z. Popovic, "A dual-band dual-output power amplifier for carrier aggregation," *IEEE Trans. Microw. Theory Techn.*, vol. 67, no. 7, pp. 3134–3146, 2019.

[9] F. Yang and Y. Rahmat-Samii, "Microstrip antennas integrated with electromagnetic band-gap (ebg) structures: a low mutual coupling design for array applications," *IEEE Trans. Antennas Propag.*, vol. 51, no. 10, 2003.

[10] B. K. Lau and J. B. Andersen, "Simple and efficient decoupling of compact arrays with parasitic scatterers," *IEEE Trans. Antennas Propag.*, vol. 60, no. 2, pp. 464–472, 2012.

[11] L. Zhao, L. K. Yeung, and K.-L. Wu, "A coupled resonator decoupling network for two-element compact antenna arrays in mobile terminals," *IEEE Trans. Antennas Propag.*, vol. 62, no. 5, pp. 2767–2776, 2014.

[12] K.-L. Wu, C. Wei, X. Mei, and Z.-Y. Zhang, "Array-antenna decoupling surface," *IEEE Trans. Antennas Propag.*, vol. 65, no. 12, 2017.

[13] J.-S. Hong and M. Lancaster, *Microstrip Filters for RF/Microwave Applications*, 1st ed. Wiley, 2001.